Paramagnetic Phospholipid-Based Micelles Targeting VCAM-1 Receptors for MRI Visualization of Inflammation.

Pagoto A[1], Stefania R[1], Garello F[1], Arena F[1], Digilio G[2], Aime S[1], Terreno E[1].

[1]Molecular & Preclinical Imaging Centers, Department of Molecular Biotechnology and Health Sciences, University of Torino , Via Nizza 52, 10126-Torino, Italy.

[2]DISIT, Università del Piemonte Orientale "A. Avogadro", Via T. Michel 11, 15121 Alessandria, Italy.

Paramagnetic phospholipid-based micelles targeting VCAM-1 receptors for the MRI visualization of inflammation

Amerigo Pagoto,[† #] Rachele Stefania, [†#] Francesca Garello, [†] Francesca Arena[†], Giuseppe Digilio[‡], Silvio Aime, [†] Enzo Terreno[†*]

[†] Molecular & Preclinical Imaging Centers, Department of Molecular Biotechnology and Health Sciences, University of Torino, Via Nizza 52, 10126 – Torino, Italy

[‡] DISIT, Università del Piemonte Orientale "A. Avogadro", Via T. Michel 11, 15121 Alessandria, Italy

*Corresponding author

Enzo Terreno,

Molecular and Preclinical Imaging Centers, Department of Molecular Biotechnology and Health Sciences, University of Torino, Via Nizza 52, 10126 – Torino, Italy.

Phone: +39-011-6706452

Fax: +39-011-6706487

e-mail: enzo.terreno@unito.it

[#] these authors contributed equally

Abstract

Inflammation is signaled by the overexpression of epitopes on the vascular endothelium that primarily aim at recruiting immune cells into the inflamed area. The intravascular localization of these biomarkers makes them suitable targets for the MRI visualization of inflammation. Phospholipid-based nanosystems appear excellent candidates in virtue of their good biocompatibility, ability to deliver a high number of imaging units at the target site, and for the easy functionalization with targeting vectors. In this work, phospholipid-based micelles (hydrodynamic diameter of 20 nm) loaded with the amphiphilic Gd(III)-complex Gd-DOTAMA$(C18)_2$ were vectorized with a small peptide able to specifically bind VCAM-1 receptors. The micelles displayed a high longitudinal relaxivity (36.4 $s^{-1}mmol_{Gd}^{-1}$ at 25°C and 0.7 T). A ^{1}H- and ^{17}O-water relaxometry study indicated that the paramagnetic complex embedded in the nanoparticles adopted two isomeric conformations, likely reflecting the well known square antiprismatic (SAP) and twisted square antiprismatic (TSAP) configurations typically observed in DOTA-like lanthanide complexes. Interestingly, the TSAP structure, showing a much faster exchange rate for the water molecule coordinated to the metal ion, was the most abundant, thus explaining the high relaxivity of the micellar agent.

The systemic administration of the micelles into a LPS-induced murine model of acute inflammation successfully demonstrated the ability of the targeting agents to detect the diseased area by T_1 contrast enhanced MRI.

Introduction

Inflammation is a complex phenomenon that implies a series of molecular and cellular modifications, such as changes in the vascular permeability and volume, infiltration and activation of both circulating leukocytes and resident immune competent cells.[1] Although the inflammatory response varies considerably with the nature of the insult, it occurs in many pathologies including atherosclerosis, cancer and diseases of the nervous system.[2-4] The activation of inflammatory cells in response to an injury is accompanied by the upregulation of endothelial inflammatory proteins, such as endothelial cell adhesion molecules (CAMs). These molecules (e.g. VCAM-1, ICAM-1, PECAM, E- and P-selectins) play an important role in the tethering, rolling, adhesion, and extravasation of immune cells, in particular leucocytes.[5,6] The molecular mechanisms responsible for specific recognition steps between activated cells and endothelium represent an intriguing opportunity for the design of imaging agents able to visualize the inflammation process. Furthermore, the intravascular localization of these epitopes makes them easily accessible for a systemically injected agent, and this feature is particularly important when signal amplification strategy is necessary to detect the target-associated imaging response.

Among CAMs, Vascular Cell Adhesion Molecule-1 (VCAM-1, member of the Ig superfamily) has been shown to be an important biomarker of several inflammatory disorders, mediating leukocyte movement across the endothelium, and its overexpression is recognized as a typical endothelial marker of inflammation,[7-9] though it has been demonstrated to be involved also in other biological events.[10] Most of the clinically available imaging techniques, namely Positron Emission Tomography (PET), Computed Tomography (CT), Ultrasound (US), and Magnetic Resonance Imaging (MRI) are currently under intense scrutiny for the design of protocols aimed at visualizing the inflammatory response.[11] In virtue of the use of non-ionizing radiations, as well as of the superb spatial resolution and ability to differentiate soft tissues, MRI is an excellent candidate to tackle this task. Moreover, MRI is often considered the technique of choice in the diagnosis of diseases with

strong inflammatory components, such as stroke and atherosclerosis.[12-14] Due to the poor sensitivity in the detection of molecular MRI agents, the search for signal amplification strategies is mandatory for the design of MR-molecular imaging protocols.[15] Typically, the increase in sensitivity is achieved by loading a high number of imaging probes (*e.g.* Gd-complexes) on macromolecular or nano/microsized carriers. These systems (especially nano/microparticles) have a limited or null blood extravasation, thus making them optimal candidates for the detection of intravascular targets.

Much efforts for the MRI visualization of inflammation have dealt with the use of agents reporting about the recruitment of immune cells in the diseased region.[16,17] Nevertheless, MR-molecular imaging of inflammation using contrast agents directed to vascular inflammatory markers is an expanding field of research and several successful examples have been already reported.[18]

In particular, VCAM-1 receptors have been exploited as MR-molecular target in experimental models of cardiovascular and neurologic diseases, and in some cases, superparamagnetic iron oxides particles were used as imaging reporting units.[19-22]

Though quite sensitive, such particles generate a T_2^*/T_2 contrast that leads to a loss of MRI signal, thus making difficult their detection in tissues with intrinsically low signal.

In this respect, contrast agents that yield a T_1 weighted signal enhancement, as Gd- or Mn-based probes, appear preferable. So far, two examples of Gd-based T_1 agents targeting VCAM-1 receptors can be found in literature. In one case, a monomeric Gd-DOTA-like complex (DOTA:1,4,7,10-tetraazacyclododecane-1,4,7,10-tetraacetic acid) was conjugated to a peptide selected by phage display showing high affinity to the target.[23] Quite unexpectedly, the presence of a single Gd per targeting vector (relaxivity of *ca.* 7.0 $s^{-1}mM_{Gd}^{-1}$ at 1.5 T and 37°C) allowed for the detection of inflamed states in mice models of hepatitis (MRI contrast enhanced by a factor of 3 with respect to the untargeted agent) and atherosclerosis (enhancement of a factor < 2 in comparison with the agent conjugated with a scrambled untargeted peptide) in mice models.

The second study dealt with rod-like nanoparticles of tobacco mosaic virus that were covalently conjugated to a VCAM-1 peptide and loaded with *ca.* 1200 units of a Gd-DOTA-like complex

(relaxivity of 14.6 $s^{-1}mM_{Gd}^{-1}$ at 1.5 T and 25°C).[24] Injected in a mouse model of atherosclerosis, this agent produced a two/threefold increase in MRI contrast when compared with both healthy mice and diseased animals administered with free Gd-DOTA.

With the aim to further improve the MRI detectability of VCAM-1 receptors using Gd-based agents, we report here a new nanosized agent based on mixed micelles made of a pegylated phospholipid, an amphiphilic Gd-complex, and a newly-synthesized phospholipid conjugated to the VCAM-1 targeting peptide (DSPE-PEG2000-peptide in Scheme 1).

We tested the *in vivo* MRI performance of the paramagnetic micelles on a LPS (lipopolysaccharide) -induced peripheral inflammation model in mice.[25]

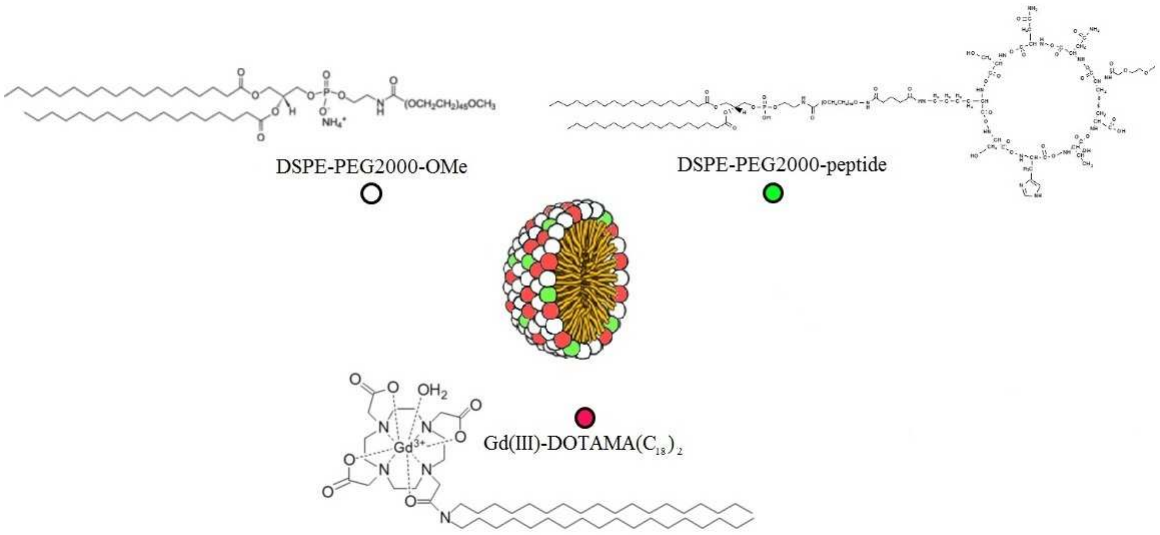

Scheme 1. Micelles composition: DSPE-PEG2000-OMe (white circle), DSPE-PEG2000-peptide (green circle), Gd(III)-DOTAMA(C_{18})$_2$ (red circle)

Results

Synthesis and characterization of DSPE-PEG2000-peptides

The VCAM-1 receptor targeting cyclic nonapeptide C*NNSKSHTC* and its untargeted scrambled version HSC*NKNSC*T were synthetized by Solid Phase Peptide Synthesis. The first aminoacids

(C and T, respectively) were attached to the resin manually, whereas the remaining amino acids were sequentially and automatically conjugated afterwards. The so-obtained linear nonapeptides were cleaved from the resin using a solution of TFA (trifluoroacetic acid) /TIPS(triisopropylsilane) /EDT (ethanedithiol) and then cyclized to obtain the final products (yield *ca.* 60%). Next, the peptides were reacted with DSG to conjugate the mono- N-hydroxy succinimide (NHS) ester at the amino group of the Lys residue of the cyclic peptides (Scheme 2). The activated NHS moiety allowed for the conjugation of DSPE-PEG2000-NH_2 to form DSPE-PEG2000-VCAM1-pep and DSPE-PEG2000-scr-pep with a yield of about 50 %.[26] The formation of the products was monitored by analytical HPLC, whereas purification was carried out by preparative HPLC using a buffered solution of ammonium acetate as eluent. The characterization of the final products was performed by ^{1}H-NMR and Mass spectrometry (see Supplementary material). A purity around 70 % was determined by analytical HPLC-ELSD for both the compounds. The remaining 30% was represented by the unconjugated phospholipid DSPE-PEG2000-NH_2 . Due to the small amount of targeting phospholipid used in the formulation, it can be assumed that the unconjugated phospholipid (whose amount was anyhow considered in the formulation of the micelles) did not interfere with the micelle formation.

Preparation and characterization of the mixed micelles

Paramagnetic mixed micelles were prepared by blending DSPE-PEG2000-OMe, DSPE-PEG2000-VCAM1-pep (or DSPE-PEG2000-scr-pep), and Gd-DOTAMA(C_{18})$_2$ in the molar ratio of 58:2:40, respectively. The hydrodynamic diameter of the micelles (determined by DLS on 3 batches) was 20 nm with a PDI of 0.2 ± 0.1. The millimolar longitudinal relaxivity (r_1) at 0.5 T of the micelles exposing the targeting peptide was 34.9 $s^{-1}mmol_{Gd}^{-1}$ at 25°C and 35.3 $s^{-1}mmol_{Gd}^{-1}$ at 37°C. The relaxivity was also measured as a function of the proton Larmor frequencies (from 0.01 to 70 MHz) and the experimental data are reported in Figure 1 (left).

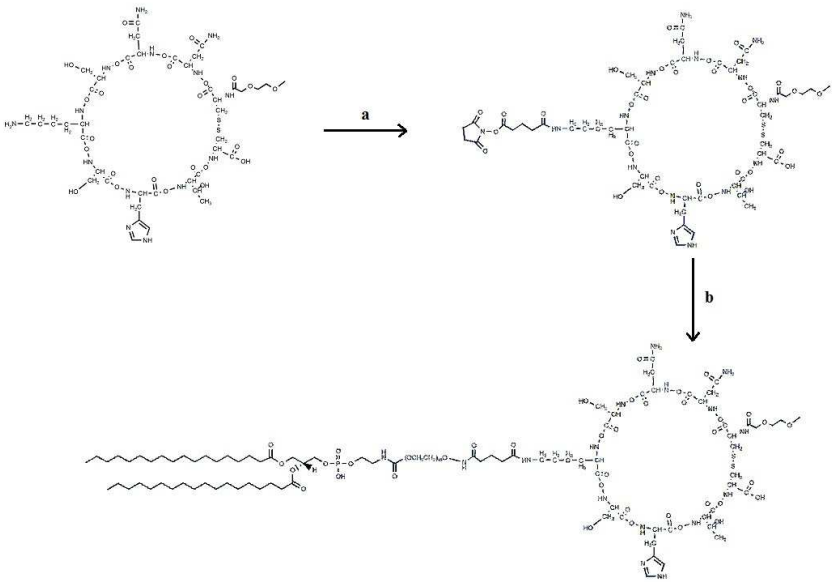

Scheme 2. Synthetic pathway to DSPE-PEG2000-VCAM1-pep. (a) DSG, DIPEA, DMF, 2 min; (b) DSPE-PEG2000-NH_2, DIPEA, DMSO, 24 h.

The obtained NMRD (Nuclear Magnetic Relaxation Dispersion) profile is characterized by a relaxivity hump at *ca.* 20-30 MHz, a feature that clearly indicates the occurrence of a restricted rotational motion for the paramagnetic Gd-complexes in the micelles.[27]

The NMRD data were complemented by the measurement of the temperature dependence of the transverse relaxation of ^{17}O-water, from which it is possible to determine the exchange lifetime, τ_M, of the water molecule coordinated to the metal centre.

Very interestingly, the data displayed a ”two-components” behaviour, thus indicating the presence of two species with very different exchange dynamics of their Gd-bound waters (Figure 1, right).[28,29] Since several parameters controlling ^{1}H and ^{17}O relaxation rates are common, NMRD and ^{17}O-data were analysed simultaneously according to the well-established Solomon-Bloembergen-Morgan and Freed theories.[27]

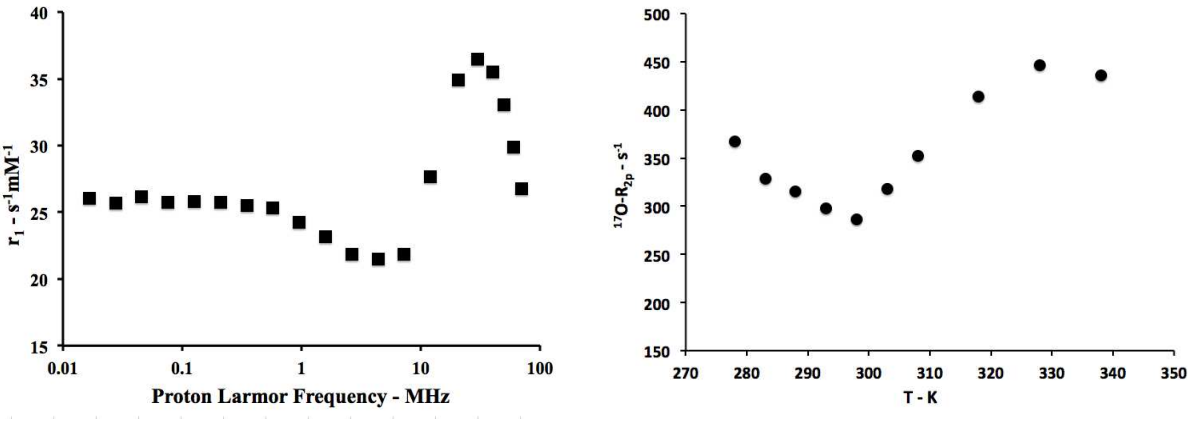

Figure 1. NMRD profile at 25°C(left) and temperature dependence of water ^{17}O-R_{2p} (right, normalized to 20 mM of Gd) of VCAM-1 targeted paramagnetic micelles.

As such theories have some limitations to properly model the behaviour of slowly tumbling systems at low Larmor frequencies,[30] NMRD data were analysed only in the high-frequency region (> 5 MHz).

The results from the fitting of experimental *vs* calculated values are reported in Table 1, whereas Figure 2 shows the fitting curves as well as the relative contributions of the two species to the measured relaxation rates.

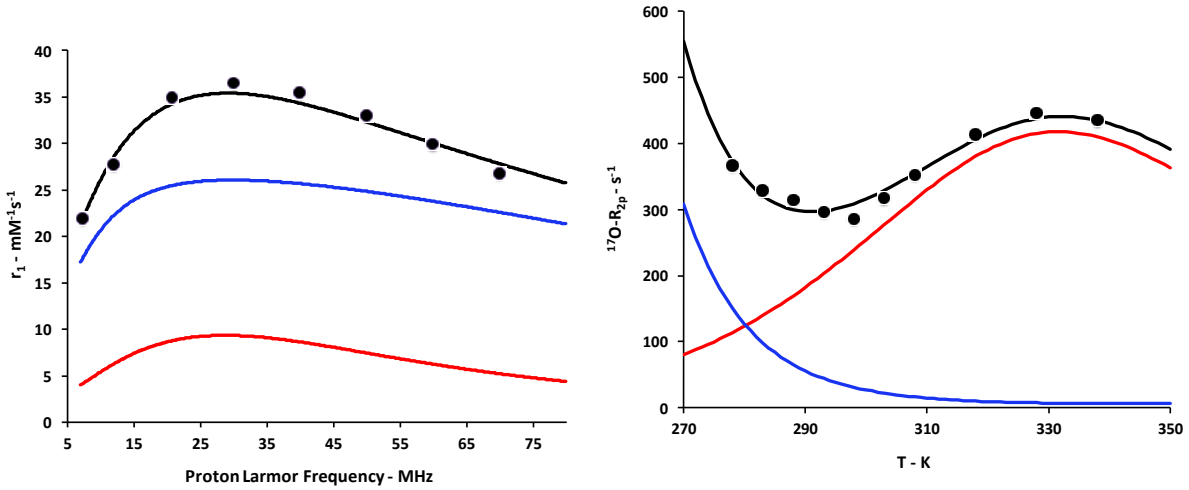

Figure 2. NMRD (left) and ^{17}O-data (right) analyzed according to the SBM-Freed theory for a system containing two species. Red and blue lines represent the contribution from species 1 and 2, respectively.

The analysis was carried out by considering Δ^2, τ_V, τ_R, τ_M, and the molar fraction of the two species (assumed to be temperature independent) as variable parameters, whereas all the other parameters were fixed to the values reported in the footnote of Table 1. As it has been reported that the hydration state (expressed by the q/r^6 value) of Gd(III) in macrocyclic conformers with different water exchange rates is inversely related to the τ_M value,[31,32] the analysis was performed using $r_{Gd\text{-}H}$ values of 3.0 Å and 3.1 Å for species 1 and 2, respectively.[31]

The good quality of the data fitting is an indirect proof that the advantages deriving from a fast water exchange rate are partially limited by a reduced hydration state.

Table 1. Values of the parameters obtained from the simultaneous fitting of NMRD and ^{17}O-R_{2p} data for the VCAM-1 targeted paramagnetic micelles. The values of τ_V, τ_R, and τ_R refer to 25°C.

Parameter	Species 1 (SAP)	Species 2 (TSAP)
$\Delta^2 \times 10^{19}$ (s^{-2})	2.2 ± 0.9	0.9 ± 0.1
τ_V (ps)	58.7 ± 4.9	41.4 ± 11.9
τ_M (ns)	380.1 ± 21.4	1.5 ± 0.2
τ_R (ns)	7.9 ± 0.8	7.5 ± 0.7
Mol. Fraction (%)	21.1	78.9

The following parameters were kept fixed during the fitting procedure: $r_{Gd\text{–}H}$ = 3.0 Å (SAP), 3.1 Å (TSAP); $r_{Gd\text{–}O}$ = 2.5 Å, $D = 2.25\times10^{-5}$ cm^2s^{-1}, q = 1, a = 3.8 Å, $A/h = -3.8\times10^6$. The activation energies related to the dynamic parameters obtained from the analysis were: $E_{\tau V}$ = 7.8 kJ/mol, $E_{\tau R}$ = 13.1 kJ/mol, $E_{\tau M}$ = 27.2 kJ/mol (SAP); $E_{\tau V}$ = 0.9 kJ/mol, $E_{\tau R}$ = 10.7 kJ/mol, $E_{\tau M}$ = 53.7 kJ/mol (TSAP).

The result of the analysis is consistent with the presence of two paramagnetic species with a predominance of the complex with a very short water exchange lifetime (species 2). The occurrence of a very short τ_M may considerably reduce the contribution of the complex to the water ^{17}O-R_{2p} values as the temperature increases. Conversely, the contribution from the complex with the slower water exchange rate (species 1) displayed a monotonic increase of ^{17}O-R_{2p} values with temperature. Therefore, in spite of the higher amount of the species 2 in the solution, ^{17}O-R_{2p} relaxation is almost exclusively determined by species 1 at physiological temperature.

On the other hand, the effect of τ_M on the proton relaxivity is quite different, and the r_1 values of the micellar agent are mainly determined by the contribution of the species 2 over the entire interval of magnetic field strengths investigated.

The *in vitro* stability of the micelles was assessed at 37°C in human serum, by measuring both size and proton relaxation rate as function of time (Figure S5). The stability of the nanoparticles was excellent and no changes in size and R_1 values were observed over a period of 5 days.

In vivo MRI testing of the paramagnetic micelles

The *in vivo* MRI performance of the micelles was tested on a murine inflammation model obtained by injecting LPS in the mouse leg skeletal muscles. Conventional H&E (hematoxylin and eosin) histology confirmed the extensive infiltration of monocytes, lymphocytes and neutrophils in the leg 48 h after LPS injection (Figure 3). Furthermore, immunofluorescence experiments confirmed the expression of VCAM-1 receptors in the inflamed muscle (Figure S6).

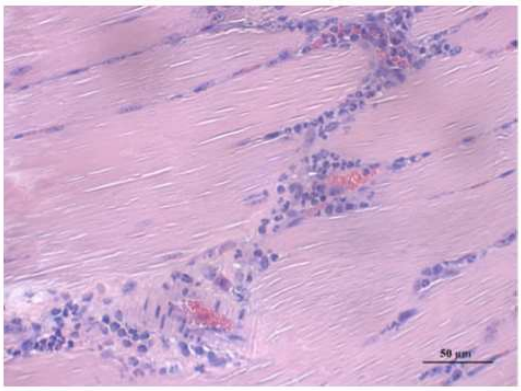

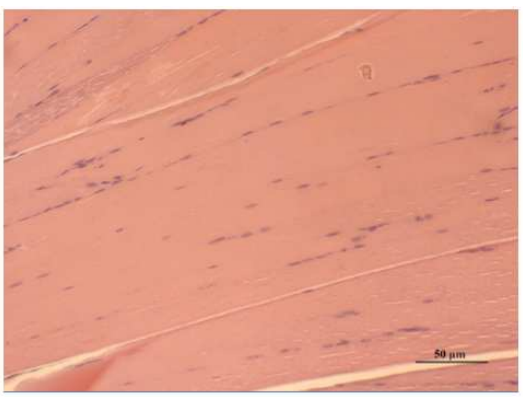

Figure 3. Histological slices stained with hematoxilin-eosin of inflamed (left) and healthy (right) leg skeletal muscle.

48 h after the induction of inflammation, the paramagnetic micelles (containing the targeting or the scrambled peptide) were injected intravenously in the tail vein at a Gd dose of 55.0 μmol/kg bw. Then, the animals (n = 6) were scanned by MRI (at 1 T) over a period of 24 h post injection. A T_1 contrast enhancement around 45 % was observed in the inflamed region 4 h post injection (Figure 4).

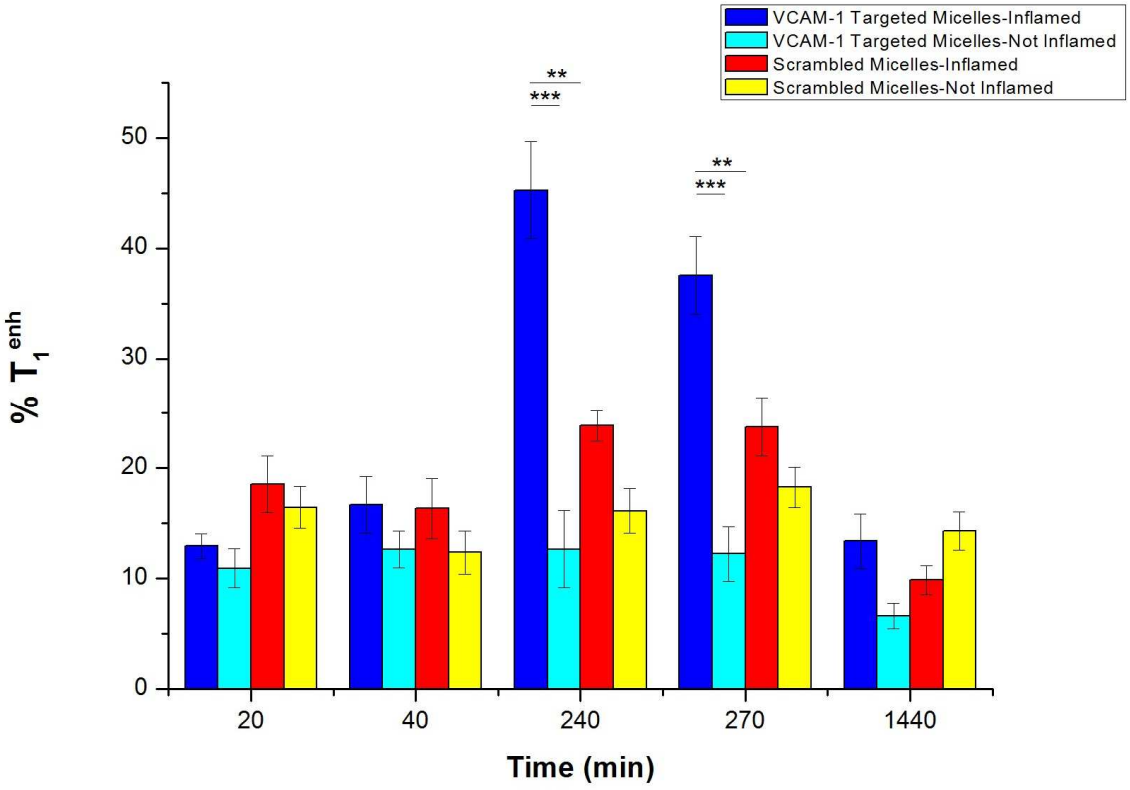

Figure 4. MRI T1 contrast enhancement at 1 T measured after intravenous injection of paramagnetic micelles. Blu bars refer to the VCAM-1 targeted micelles on inflamed leg while red bars to the control experiment (scrambled peptide) on inflamed leg. Cyan and yellow bars refer to targeted and control micelles on healthy leg, respectively (*** $p < 0.01$ - ** $p < 0.05$). Error bars represent SE (Standard Error) on mean (n = 6).

The contrast measured in the inflamed leg was *ca.* fivefold higher than the enhancement detected in the contralateral healthy leg, and twofold higher than the response measured upon administration of the control micelles functionalized with the scrambled peptide. The MR images reported in Figure 5 show that 4 h after the injection of the micelles, an hyperintense signal was visible in the inflamed leg (red circle), while no brightening was detected in the control experiment.

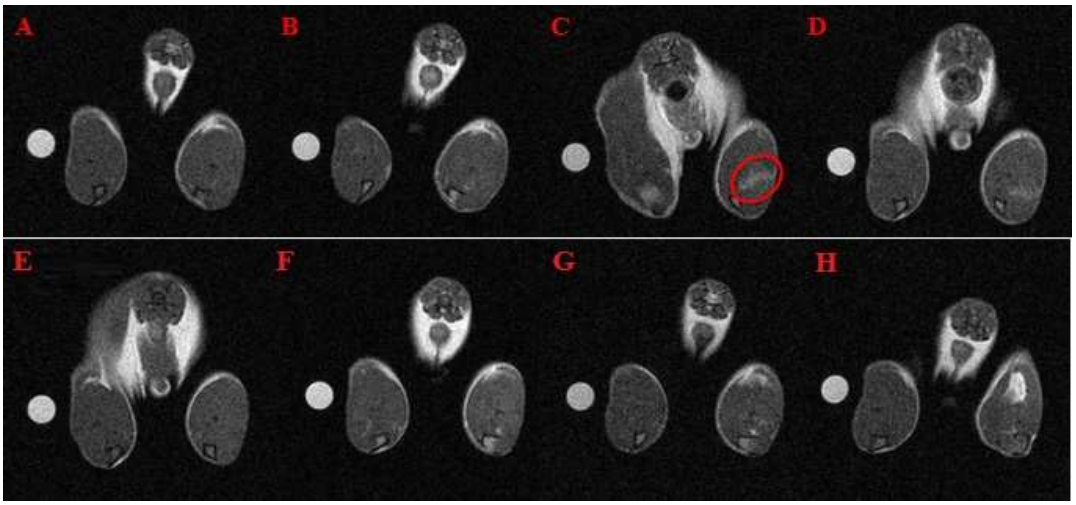

Figure 5. Axial T_{1w} MR images of the legs of C57BL/6J mice acquired pre (A, E) , 40 min (B, F), 4 h(C, G) and 24 h (D, H) after the injection of micelles targeting VCAM-1 receptors (top row) or micelles loaded with the scrambled peptide (bottom row). LPS was injected in the right leg muscle. The red oval highlights the inflamed area detected with the targeted agent.

Besides the inflamed legs, a significant MRI contrast was also detected in liver, spleen and kidneys even 24 hours after the injection of the micelles (Figure S7).

The accumulation of the MRI agent in the legs was confirmed by ICP-MS analysis (Figure 6), which showed that the amount of metal ion in the inflamed muscles after the injection of the VCAM-1-targeted micelles was ca. 40 % higher than the amount found in the diseased tissue after the injection of the control micelles loaded with the scrambled peptide, and *ca.* threefold higher with respect to the Gd found in the healthy muscles regardless of the type of micelles injected.

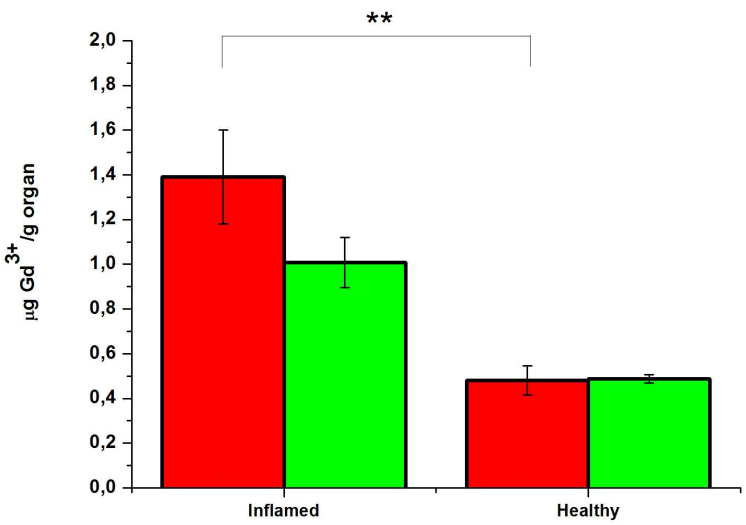

Figure 6. Amount of Gd (normalized to the organ weight) measured in legs excised 4 h after the intravenous injection of paramagnetic micelles. Red: VCAM-1 targeted agent, Green: control agent. Error bars refer to the SE on mean (n = 6).

Discussion

The primary motivation of this work was to develop an improved MRI T_1 Gd-based agent for targeting the intravascular VCAM-1 receptors, as biomarker of endothelium activated by inflammation.

The most straightforward approach to increase the detection sensitivity of MRI contrast is to load a high number of paramagnetic centers to a nanocarrier suitably designed to bind the desired target. The loading of the agent to the carrier invariably slows down the rotational motion of the paramagnetic complex, and, consequently, it can markedly affect the magnetic field dependence of the relaxivity of the system. In particular, an increase in sensitivity occurs in a field range between 0.2 and 1.5 T, mainly depending on the exchange rate of the Gd-bound water protons, and the electronic relaxation times of the paramagnetic center.

Though several hints to design Gd(III) complexes with high relaxivity at fields exceeding 1.5 T have been already proposed,[33,34] the simplest approach to increase the sensitivity relies on: *a*) the

use of thermodynamically and kinetically stable Gd-agents (possibly already validated *in vivo)*, *b*) their loading into a biocompatible targeted carrier, and *c*) the detection of the contrast on a MR scanner operating at a magnetic field chosen to maximize the relaxometric properties of the agent.

Steps *a* and *b* are somehow related because the choice of the Gd-agent may be influenced by the physico-chemical properties of the carrier. In this work, we decided to use phospholipid-based micelles for their high biocompatibility and favorable pharmacokinetic properties. The easiest way to load a MRI agent in these soft self-aggregates is through the design of a metal complex with a phospholipid-like structure, *i.e.* characterized by the presence of a lipophilic portion conjugated to the hydrophilic coordination cage hosting the paramagnetic metal.

The complex Gd-DOTAMA(C_{18})$_2$ perfectly meets this requirement, and it was already successfully used in many literature reports, mostly incorporated in bilayered membranes of liposomes.[35-37] Though the presence of an amidic coordinating group does not guarantee an optimal exchange rate of the water molecule bound to the metal, the thermodynamic and kinetic stabilities of the complex, as well as the efficiency and stability of the loading to lipid-based particles, are very good, thus making this agent an excellent option for the preparation of MRI detectable nanocarriers.

In addition to the MRI probe, micelles were also loaded with a newly synthesized phospholipid-based peptide for targeting VCAM-1 receptors. The peptide, selected by phage display by others,[23] was prepared by solid phase synthesis and then conjugated at the polar distal end of the phospholipid DSPE-PEG2000. In parallel, a non-targeted scrambled version of the peptide was synthesized, conjugated with the same phospholipid, and used to prepare paramagnetic micelles acting as control for the *in vivo* imaging experiments.

The shape of the NMRD profile measured for the paramagnetic micelles (Figure 1, left) was fully consistent with the occurrence of a restricted rotational motion for the Gd-complex embedded in the nanoparticle. The relaxivity reached a maximum value of 36.4 $s^{-1}mM_{Gd}^{-1}$ at the Larmor frequency of 30 MHz (and 25°C), *i.e.* about fivefold larger than the corresponding value measured for the

monomeric agent reported in ref. 23, and 2.5 times higher than the r_1 value reported for nanosized agent based on the tobacco mosaic virus.[24]

In the latter system, a number of *ca.* 1200 Gd-complexes per particle was estimated, which led to a particle relaxivity of 17520 $s^{-1}mM^{-1}$. We made a rough calculation of the number of Gd-DOTAMA(C_{18})$_2$ units loaded into a single micelle on the basis of the area occupied by the two main components (DSPE-PEG2000 and Gd-DOTAMA(C_{18})$_2$, see Experimental Procedures). Considering a molecular surface area of 0.45 nm^2 and 0.8 nm^2 for DSPE-PEG2000 and Gd-DOTAMA(C_{18})$_2$, respectively,[36,38] and using the average particle radius obtained by DLS measurements (10 nm), *ca.* 850 Gd-complexes resulted to be loaded in a single micelle, which corresponds to a particle relaxivity of about 30000 $s^{-1}mM^{-1}$, with an improvement of *ca.* 70 % with respect to the agent reported in ref. 24.

Interestingly, the temperature dependence of water ^{17}O-R_{2p} (Figure 1, right) clearly indicated the presence of two paramagnetic species in the micelles suspension, characterized by very different water exchange rates.

This behavior, which was observed in a series of trans-bisamide derivatives of Gd-DOTA[28] and more recently even for Gd-HPDO3A,[29] can be interpreted in terms of the presence of comparable amounts of the two conformational isomers of Ln-DOTA complexes with capped square antiprismatic (SAP) and capped twisted square antiprismatic (TSAP) structure.[39]

It has been clearly demonstrated that the two isomeric configurations display different exchange rates for the water molecule occupying the capped position, being the TSAP isomer the structure with the faster exchange.[40,41]

The simultaneous analysis of NMRD and ^{17}O-R_{2p} data for the paramagnetic micelles investigated in this work allowed the estimation of the residence lifetime (τ_M) for the Gd-bound water molecule in the two species that resulted to be 380 ns and 1.5 ns for SAP and TSAP isomers, respectively (Table 1). Therefore, it is straightforward to assign the species with the larger τ_M value to the SAP conformation and that one with the faster exchange to the TSAP structure. The ratio between the τ_M

values for the two diastereoisomers (about 310) lies in the middle of the range reported in literature for Gd-DOTA bisamide complexes (100-700).[28] However, likely due to the electroneutrality of Gd-DOTAMA(C_{18})$_2$ complex, the exchange lifetime for both the isomers incorporated in the micelles is almost an order of magnitude lower than the mono-positively charged bisamide derivatives.

Due to the water insolubility of Gd-DOTAMA(C_{18})$_2$, it was not possible to assess if the distribution (21.8% SAP and 78.2 % TSAP as obtained from the relaxometric analysis) and water dynamics of two isomers are influenced by the inclusion of the amphiphilic complex in the nanoparticle. Actually, effects of the characteristics of the local microenvironment on the isomer distribution in DOTA-amide complexes have been already reported.[42] It is interesting to note that, unlike other macrocyclic complexes, the SAP/TSAP ratio for Gd-DOTAMA(C_{18})$_2$ in micelles is lower than 1. This finding is very important because the occurrence of a short water residence lifetime allows the attainment of high relaxivities especially when (as in this case) the Gd-complex experiences a slow rotational motion.

The different water exchange regime for the two conformations likely accounts for the very similar r_1 values (at 0.5 T) measured at 25°C (34.9 $mM^{-1}s^{-1}$) and 37 °C (35.3 $s^{-1}mM^{-1}$), respectively.

The NMRD profile clearly identifies the range of magnetic field where the micelles display the best performance to generate MRI contrast and, on this basis, the *in vivo* testing was performed at 1 T (corresponding to a Larmor frequency of 42.5 MHz).

The agent was validated *in vivo* on an inflammation model obtained upon intramuscular injection of LPS in mice leg. The effective onset of inflammation 48 hours after LPS injection was confirmed histologically (Figure 3).

The paramagnetic micelles were intravenously injected at a dose of 55.0 μmol Gd/kg bw, and the animals were monitored by MRI at different times (20 min, 40 min, 4 h, 4.5 h, and 24 h) post injection. The data shown in Figure 4 indicated that the micelles targeting VCAM-1 receptors yielded a maximum contrast enhancement (*ca.* 45 %) 4 h post-injection. Such a contrast was *ca.* fivefold higher than the response observed in the healthy contralateral leg, and *ca.* twofold higher

than the contrast measured upon injection of the control micelles loaded with the scrambled peptide. Likely, the difference in the contrast observed between the diseased and the healthy leg after the injection of the control micelles (also observed in ref. 23) can be ascribed to a non-specific accumulation of the untargeted probe in the lesion.

The different contrast enhancement measured *in vivo* was confirmed by the amount of Gd determined in the explanted muscles by ICP-MS. The data obtained (shown in Fig. 6) paralleled the trend observed for the MRI contrast, thus highlighting the superior accumulation of the targeted agent in the inflamed region. However, the difference observed among the experimental groups in the ICP-MS analysis was smaller than MRI contrast (*e.g.* the 40 % difference between the amount of Gd found in the inflamed muscles in targeted and control groups was not statistically significant). This is likely the result of the different contribution of the inflamed tissues in the two experiments. In fact, while it was possible to calculate the MRI contrast mostly in the inflamed area, the amount of Gd was determined over the whole explanted muscle, thus diluting the difference with the control group.

In conclusion, this work proposes a new highly sensitive MRI nanoagent for the *in vivo* visualization of inflammation through the targeting of the intravascular VCAM-1 receptors. The system derives by the self-assembling of natural phospholipids (or partly conjugated with a VCAM-1 directed peptide) and an amphiphilic Gd-complex, which forms micelles with a diameter of *ca.* 20 nm. The combination between the high relaxivity displayed by the single contrastophore and the high number of complexes loaded per micelle makes this agent suitable to overcome the sensitivity issue often associated with MR-molecular imaging experiments. However, the favorable property of this agent can be fully exploited only if it is imaged at a magnetic field tuned with the NMRD profile of the system (here 0.5-1.5 T). When injected *in vivo* in a mouse model of acute inflammation and monitored at 1 T, the agent performed very well allowing the detection of a contrast about fivefold higher than that one measured in the non inflamed tissue.

We expect that the herein reported results will stimulate researches to further assess and optimize the pharmacokinetic properties with the ultimate goal to develop a clinical-translatable MRI agent for diagnostic/theranostic protocols on inflammation-associated diseases.

Experimental Procedures

Chemicals

1,2- distearoyl-*sn*-glycero-3-phospho-ethanolamine-N-[amino(poly-(ethylene glycol)2000] ammonium salt (DSPE-PEG2000-NH2), 1,2-distearoyl-*sn*-glycero-3-phosphoethanolamine-N-[methoxy(polyethylene glycol)-2000] ammonium salt (DSPE-PEG2000-OMe)were obtained from Avanti Polar Lipids (Alabaster,USA). Gd-DOTAMA(C_{18})$_2$ was synthesized as described elsewhere.[43] Disuccinimidyl glutarate (DSG) was prepared in-house from glutaric acid and NHS.

Synthesis of the targeting peptide and its scrambled version

The peptides C*NNSKSHTC* and HSC*NKNSC*T were synthesized on Liberty CEM microwave peptide synthesizer using H-Cys(*Trt*)-2-chlorotrityl resin and standard FMOC (fluorenylmethyloxycarbonyl chloride) chemistry.

The attachment of the first amino acid Fmoc-Cys-(Trt)-OH or Fmoc-Tyr(tBu)-OH to 2-chlorotrityl chloride resin to give H-Cys(Trt)-2-chlorotrityl resin was carried out as follows:

Fmoc-Cys-(Trt)-OH (3.28 g, 5.6 mmol) or Fmoc-Tyr(tBu)-OH (2.76 g, 6 mmol) was dissolved in 5 ml of DCM (dichloromethane) and then added with DIPEA (diisopropylethylamine) (0.896 ml, 5.12 mmol). The mixture was stirred for 10 minutes. While under stirring, 2-Chlorotrityl chloride resin (2.0 g, 2.24 mmol,) was added. The resulting mixture was continuously stirred for 3 hours. The resin was filtered and washed with DCM (10 ml×6 washings 3 min each). The resin was capped with MeOH (methanol):DIPEA (5:1, 10 ml×3 times) for 5 min. The resin was first washed with DMF (dimethylformamide) (10ml×6 times, 3 min each) and then in DCM (10 ml×3 times, 3 min

each). Next, the resin was dried for 12 hours under high vacuum. Yield > 90%. Substitution: 0.59 mmoles/g.

The remaining amino acids were coupled automatically by using 5.0 equivalents excess of Fmoc-amino acids, 5 min at 75 °C, 35 Watt, in presence of PyBOP (benzotriazol-1-yl-oxytripyrrolidinophosphonium hexafluorophosphate), DIPEA in DMF and the Fmoc-deprotection steps (20% piperidine in DMF) were completed within 3 min at 75 °C.

The cleavage from the resin was pursued with TFA/ TIPS/ EDT (95:3:2, v:v) for 2 h at room temperature. The peptide was then precipitated and washed with diethyl ether. The obtained solid was dissolved in water with 5% of DMSO (dimethyl sulfoxide) and stirred for 24 h to afford the cyclization of the two Cys residues within the peptides. The solution was lyophilized to give the final product (166 mg, yield 61%, Purity = 91% for C*NNSKSHTC* and 72 mg, yield 65 %, purity 92 % for HSC*NKNSC*T).

Analytical HPLC-MS was carried out on a Waters Fraction Lynx autopurification system equipped with micromass ZQ (ESCI ionization mode and dual-λ detectors), column Waters Atlantis RP-C18, 5 μm, 4.6 mm × 150 mm, eluents A, H_2O(0,1 % TFA); B, CH_3CN (0,1% TFA), elution initial condition 5% B, linear gradient 5-10% B over 2.49 min, 10-15% B over 15 min, flow rate 1 ml/min, UV detection at 220 nm. t_R= 8.4 min, MS-ESI(+) m/z: 1107$[M+H]^+$, 554$[M+2H]^{2+}$, calculated for $C_{41}H_{66}N_{14}O_{18}S_2$ =1106. The corresponding data for HSC*NKNSC*T were t_R= 9.4 min, MS-ESI(+): m/z: found: 1106$[M+H]^+$, 554$[M+2H]^{2+}$ calculated for $C_{41}H_{66}N_{14}O_{18}S_2$ = 1106.

Peptides were also characterized by ^{1}H-NMR and 2D-TOCSY, NOESY and COSY spectra in H_2O (0.550 ml) - D_2O (0.050 ml) at pH 5 and room temperature. NMR spectra were recorded on Bruker Avance 600 spectrometer and analyzed using the Computed Aided Resonance Assignment software (The Swiss Federal Institute of Technology, Zurich, Switzerland) (Figure S1 and Table S1).

Preparation and purification of DSPE-PEG2000-Peptide

A solution of the cyclic nonapeptide (0.020 g, 0.017 mmol) dissolved in anhydrous DMF (1.0 mL) was added to a solution of DSG (41.0 mg, 0.128 mmol) dissolved in anhydrous DMF (0.5 mL) containing DIPEA (0.057 mL, 0.34 mmol, 20 equivalent), and the solution was vigorously shaken for 2 min. The reaction mixture was stirred for 5 min. Then, 10 mL of ethyl acetate was added to the reaction mixture and the precipitate, corresponding to the glutaric acid monoamide mono-NHS ester of the peptides, was centrifuged to a pellet and washed twice with ethyl acetate (10 mL). A solution of this product in anhydrous DMSO (0.5 mL) containing DIPEA (0.050 mL, 0.3 mmol, 20 equiv), was added to a DMSO solution (0.5 mL) of DSPE-PEG2000-NH_2 (0.021 g, 0.0075 mmol, 0.5 equiv.), and the mixture was stirred at room temperature. The reaction was monitored by analytical HPLC and reached the completeness after 24 h. The reaction mixture was added with 10 ml of water and then lyophilized. The products were purified by preparative HPLC using Waters XTerra RPdC8, 19/100 column, 7 mM CH_3COONH_4 (A) e CH_3CN (B) as eluents, initial condition 40 % B, 40-80 % B in 2.45 min, 80-90 % B in 7 min, flow rate 20 ml/min.

Analytical HPLC: t_R= 17.55 min., purity 70 %, column Fluofix 120 E (4.6 mm ×250 mm), eluents: A, H_2O; B, ethanol: isopropyl alcohol 70:30 (v/v), elution, initial condition 20% B, isocratic gradient 20% B in 5 min, 20-80 % B in 20 min, 80-100 % B in 3 min, flow rate 1.2 ml/min, column temperature 40°C, ELSD detection (temp 45°C, pressure 35 atm).

C*NNSKSHTC*: MS-MALDI–TOF: m/z: 4017 calcd $C_{178}H_{333}N_{16}O_{74}PS_2$ = 3974.

HSC*NKNSC*T: MS-MALDI–TOF: m/z: 4005 calcd $C_{178}H_{335}N_{17}O_{74}PS_2$ = 3977.

MS spectra are reported in Figures S2, S3, and S4.

Mixed micelles preparation

Micelles were formulated with DSPE-PEG2000-OMe, Gd-DOTAMA(C_{18})$_2$ and DSPE-PEG2000-VCAM1-pep (or scr) in a molar ratio of 58:40:2 respectively. The mixture (total amount 22.5 mg) was dissolved in chloroform and MeOH (4:1 v/v), and the solution was slowly evaporated (30°C) to

form a thin film on the bottom of a flask. The film was hydrated at 50 °C for 10 min adding 1.5 ml of HEPES-buffered saline (pH 7.4, 38 mM of HEPES, 0.15 M of NaCl). The suspension was sonicated twice for 90 sec (power 70%, Sonicator Bandelin Sonoplus HD 2070, Berlin, Germany). During the sonication the mixture was cooled with ice to keep the temperature under 10°C.

Micelle characterization

The millimolar longitudinal relaxivity (r_1) of the paramagnetic nanoparticles was measured at 0.5 T (Stelar Spinmaster Spectrometer, Pavia, Italy). The concentration of Gd(III) in the micelles suspension was determined by relaxometry.[44] The mean hydrodynamic diameter of the particles was determined using Dynamic Light Scattering (Malvern ZS Nanosizer, UK) with a scattering angle of 90°C. The polydispersion index (PDI) was used as indicator of the particle size distribution. Micelle stability was investigated monitoring longitudinal relaxivity and size over 5 days (DLS) and 15 days (relaxometry) in human serum (HS, SERO, Billingstad, Norway). The relaxation rate of the micelles-containing suspension was also measured at 25°C over magnetic field strengths ranging from 7 to 20 MHz (Spinmaster FFC2000 1T C/DC, Stelar, Mede (PV), Italy). Additional values at higher Larmor frequencies (30-70 MHz) were obtained with a tunable relaxometer (Spinmaster, tunable magnet, Stelar, Mede (PV), Italy). Temperature was controlled with a Stelar VTC-91 airflow heater equipped with a calibrated copper−constantan thermocouple (uncertainty of ±0.1 K). Variable-temperature ^{17}O NMR measurements were recorded on a Bruker Avance 600 spectrometer equipped with a 5 mm probe and standard temperature control unit. The micelle suspension contained 2.0% of ^{17}O water (Cambridge Isotope).

The observed transverse relaxation rates were calculated from the signal width at half-height.

The paramagnetic contribution was calculated using a suspension of Gd-free micelles.

The number of Gd(III)-complexes loaded in a single micelle was estimated as follows:

$$n_{micelle}^{Gd} = \frac{n_T^{Gd}}{n_T^{micelle}} \qquad [1]$$

where n_T^{Gd} and $n_T^{micelle}$ represent the total number of Gd-complexes and particles, respectively. $n_T^{micelle}$ can be obtained from the ratio between the total surface area of the micelles (A_T) over the surface of the single, spherical, particle:

$$n_T^{micelle} = \frac{A_T}{A_{\text{sin}\,gle}} = \frac{A_T^{Gd} + A_T^{DSPE}}{4\pi r^2} = \frac{mol^{Gd} N_{AV} A^{Gd} + mol^{DSPE} N_{AV} A^{DSPE}}{4\pi r^2} \qquad [2]$$

where $mol^i N_{AV}$ terms refer to the number of Gd-complexes (i = Gd) and DSPE molecules (i = $DSPE$) in a given micelles suspension, A^i values represent the molecular surface areas for the two components, and r is the average particles radius (N_{AV} is the Avogadro's constant).

Under the assumption that the molar ratio between the micelle components does not vary during the preparation:

$$mol^{DSPE} = mol^{Gd} \frac{\%^{DSPE}}{\%^{Gd}} \qquad [3]$$

where $\%^i$ represents the molar ratio of the i component in the formulation (in this work 40 % and 60 % for Gd-DOTAMA(C_{18})$_2$ and DSPE-PEG2000, respectively).

Eq. 1 can be rearranged considering Eqs. 2-3 and substituting n_T^{Gd} with $mol^{Gd} N_{AV}$:

$$n_{micelle}^{Gd} = \frac{mol^{Gd} N_{AV}}{\frac{mol^{Gd} N_{AV} A^{Gd} + mol^{Gd} \frac{\%^{DSPE}}{\%^{Gd}} N_{AV} A^{DSPE}}{4\pi r^2}} = \frac{4\pi r^2}{A^{Gd} + \frac{\%^{DSPE}}{\%^{Gd}} A^{DSPE}} \qquad [4]$$

Animal model

C57BL/6J male mice (20–25 g) were divided into two groups: A) LPS inflamed mice receiving the targeted micelles (n=6), and B) LPS inflamed mice receiving the untargeted micelles exposing the scrambled peptide (n=6). The inflammation was induced in the right calf muscle by intramuscular injection of 100 µl of LPS 0.5 mg/mL in PBS (phosphate buffer saline) (LPS, Escherichia coli 055:B5) under 1.5% isoflurane anesthesia. In control mice 100 µl PBS were injected in the right calf muscle. Animals were recruited for MRI 48 h after LPS injection. The model was validated histologically. To this purpose, 48 h post LPS injection, right and left legs were excised and

immediately cryopreserved in Optimum Cutting Temperature (O.C.T.) compound (VWR International) (5 min in liquid nitrogen before cooling down to -80°C). Slices (thickness 5 μm) were cut using a cryostat (Leica CM 1950) and fixed in formalin for 10 min. Sections were then hydrated, stained with hematoxylin and eosin and dehydrated to be mounted with a coverslip. Images of the samples were obtained by using the Olympus BH2 optical microscope.

Animal manipulation and experimental procedures were carried out in accordance with the European Community guidelines, and under the approval of the Italian Ministry of Health.

Immunofluorescence

Indirect immunofluorescent detection and localization of VCAM-1 receptors were performed. Sections (5-μm thick) of the leg muscles were cut with a cryostat (Leica CM 1950) and then fixed with ethanol 99% at room temperature for 8 min and washed with PBS. To block nonspecific binding sites, sections were incubated for 1 h with 10% BSA (Bovine Serum Albumin) in PBS. Sections were then incubated with primary Ab (ab24853 – Abcam) at 4°C (diluted 1:200 for VCAM-1 in PBS containing 10% BSA) overnight. After three washings with PBS, sections were incubated for 60 min with FITC-tagged goat anti-rat IgG (35552 - ThermoFisher) (1:500 dilution in PBS) at room temperature. After washings with PBS, sections were stained with Hoechst (33342 – Sigma) (1:10000 dilution in PBS for nuclear staining). After fast (5 min) washing in bidistilled water, the sections were mounted with ProLong (ThermoFisher) antifade mountant. Microscopic observation and image acquisition were performed with a Leica TCS SP5 confocal microscope (Leica Microsystems s.r.l.).

In vivo MRI experiments

48 h post LPS injection, 200 μL of a suspension of targeted or untargeted micelles (0.055 mmol Gd/kg bw) were intravenously administered to C57BL/6J mice. MRI was performed before and

then 20 min, 40 min, 4 h, 4.5 h, and 24 h after micelle injection on a Bruker Icon (1 T). A RARE sequence with the following acquisition parameters was used: TR/TE = 380/14.7 ms, matrix = 256, no. of averages = 6, FOV = 5 cm, slice thickness = 1.5 mm, 121 axial slices, TA = 254 s). Mice were kept under isoflurane anaesthesia during the image acquisition.

ICP-MS measurements

ICP-MS (Thermo Scientific ELEMENT 2 ICP-MS -Finnigan, Rodano, Milano, Italy) was used to quantify Gd (III) on explanted tissues. Inflamed and contralateral healthy muscles of mice injected with the micelles were resected 4 h post injection. The specimens were digested in nitric acid (1 mL) and then mineralized at 160°C under microwave heating (Milestone MicroSYNTH Microwave labstation equipped with an optical fiber temperature control and HPR-1000/6M six position high-pressure reactor, Bergamo, Italy).

Image processing and analysis

Image analysis was performed using Bruker ParaVision 4.0 software. Regions of interest (ROIs) were manually drawn over the inflamed and controlateral healthy leg in all the axial imaging slices and the average signal intensity was calculated. The % T_1 contrast enhancement at a given time after administration ($\%T_1^{enh}{}_{(t)}$) was obtained as follows:

$$\%T_1^{enh}{}_{(t)} = \frac{S_{(t)}^{POST} - S^{PRE}}{S^{PRE}} \times 100$$

where S^{PRE} and $S_{(t)}{}^{POST}$ represent the average signal before and after the injection of the contrast agent, respectively.[35] p values were calculated using t-Student's test, assuming statistical significance at $p < 0.05$ and $p < 0.01$.

Acknowledgements

The financial support from the EU-FP7 collaborative project INMiND (Imaging Neuroinflammation in neurodegenerative diseases, http://www.uni-muenster. de/InMind) is gratefully acknowledged. We thank Prof. Juan Carlos Cutrin for his valuable assistance in the histological analysis.

Abbreviation

BSA, bovine serum albumin; COSY, correlation spectroscopy; DCM**,** dichloromethane; DIPEA, diisopropylethylamine; DLS, dinamic light scattering; DMF dimethylformamide; DMSO, dimethyl sulfoxide; EDT, ethanedithiol; ELSD, evaporative light scattering detector; FMOC, fluorenylmethyloxycarbonyl chloride**;** H&E, hematoxylin-eosin; HPLC, high performance liquid chromatography; ICP-MS, inductively coupled plasma mass spectrometry; LPS, lipopolysaccharide; MALDI – TOF, matrix assisted laser desorption ionization – time of flight; MeOH, methanol; MS-ESI, mass spectroscopy – electrospray ionization; NOESY, nuclear overhauser effect spectroscopy; NMRD, nuclear magnetic relaxation dispersion; PBS, phosphate buffer saline; PyBOP, benzotriazol-1-yl oxytripyrrolidinophosphonium hexafluorophosphate; SAP, square antiprismatic; SE, standard error; TFA, trifluoroacetic acid; TIPS, triisopropylsilane; TOCSY, total correlation spectroscopy; TSAP, twisted square antiprismatic; VCAM, vascular cell adhesion molecule;

References

1.Ryan GB and Majno G. (1977) Acute inflammation. A review. *Am J Pathol*. 86,183-267

2. Libb P, Ridker PM, Maseri A. (2002) Inflammation and Atherosclerosis. Circulation;105**,**1135-1143

3. Grivennikov SI, Greten FR, and Karin M. (2010) Immunity, Inflammation, and Cancer. *Cell.* 140**,**883-899.

4. Xanthos DN and Sandkühler J. (2014) Neurogenic neuroinflammation: inflammatory CNS reactions in response to neuronal activity. *Nature Reviews Neuroscience*. 15,43-53.

5. Gahmberg CG, Tolvanen M, Kotovuori P. (1997) Leukocyte adhesion, Structure and function of human leukocyte P,-integrins and their cellular ligands. *Eur J Biochem*. 245,215-232.

6. Carlos TM and Harlan JM. (1994) Leukocyte-Endothelia1 Adhesion Molecules. *Blood.* 7**,** 2068-2101.

7. Blake GJ and Ridker PM. (2002) Inflammatory bio-markers and cardiovascular risk prediction. *Journal of Internal Medic*ine. 4,283-294

8. Blake GJ and Ridker PM. (2001) Novel Clinical Markers of Vascular Wall Inflammation. *Circulation Research*. 89,763-771.

9. Cook-Mills JM, Marchese ME, Abdala-Valencia H. (2011) Vascular Cell Adhesion Molecule-1 Expression and Signaling During Disease: Regulation by Reactive Oxygen Species and Antioxidants. *Antioxidants & Redox Signaling* 15, 1607-1638.

10. Dean DC, Iademarco MF, Rosen GD, Sheppard AM. (1993) The Integrin $\alpha_4\beta_1$ and Its Counter Receptor VCAM-1 in Development and Immune Function. *Am. Rev. Respir. Dis.* 148, S43-S46.

11. Jacobs AH, Tavitian B and the INMIND consortium. (2012) Noninvasive molecular imaging of neuroinflammation. *J Cereb Blood Flow Metab*. 32,1393-1415.

12. Deddens LH, van Tilborg GA, van der Toorn A, van der Marel K, Paulis LE, van Bloois L, Storm G, Strijkers GJ, Mulder WJ, de Vries HE, Dijkhuizen RM. (2013) MRI of ICAM-1

Upregulation After Stroke:the Importance of Choosing the Appropriate Target-Specific Particulate Contrast Agent. *Mol Imaging Biol*. 15, 4114-4122.

13. Baird AE and Warach S. (1998) Magnetic resonance imaging of acute stroke. *J Cereb Blood Flow Metab*. 18,583-609.

14. Corti R and Fuster V. (2011) Imaging of atherosclerosis: magnetic resonance imaging. *European Heart Journal*. 32,1709-1719b.

15. Caravan P (2006) Strategies for increasing the sensitivity of gadolinium based MRI contrast agents. *Chemical Society Reviews*. 35,512-523.

16. Beckmann N, Cannet C, Babin AL, Blé FX, Zurbruegg S, Kneuer R, Dousset V. (2009) In vivo visualization of macrophage infiltration and activity in inflammation using magnetic resonance imaging. *Wiley Interdiscip. Rev. Nanomed. Nanobiotechnol.* 1:272-298.

17. Stoll G, Basse-Lüsebrink T, Weise G, Jakob P. (2012) Visualization of inflammation using (19)F-magnetic resonance imaging and perfluorocarbons. *Wiley Interdiscip. Rev. Nanomed. Nanobiotechnol.* 4:438-447.

18. Chacko AM, Hood ED, Zern BJ, and Muzykantov VR (2011) Targeted Nanocarriers for Imaging and Therapy of Vascular Inflammation, *Curr Opin Colloid Interface Sci*. 16**,**215-227.

19. Burtea C, Ballet S, Laurent S, Rousseaux O, Dencausse A, Gonzalez W, Port M, Corot C, Vander Elst L, Muller RN.(2012) Development of a magnetic resonance imaging protocol for the characterization of atherosclerotic plaque by using vascular cell adhesion molecule-1 and apoptosis-targeted ultrasmall superparamagnetic iron oxide derivatives. *Arterioscler Thromb Vasc Biol* 32, 36-48.

20. Michalska M, Machtoub L, Manthey HD, Bauer E, Herold V, Krohne G, Lykowsky G, Hildenbrand M, Kampf T, Jakob P, Zernecke A, Bauer WR. (2012) Visualization of vascular inflammation in the atherosclerotic mouse by ultrasmall superparamagnetic iron oxide vascular cell adhesion molecule-1-specific nanoparticles. *Arterioscler Thromb Vasc Biol*. 32, 2350-2357.

21. Gauberti M, Montagne A, Marcos-Contreras OA, Le Béhot A, Maubert E, Vivien D. (2013) Ultra-sensitive molecular MRI of vascular cell adhesion molecule-1 reveals a dynamic inflammatory penumbra after strokes. *Stroke*. 44, 1988-1996.

22. Patel N, Duffy BA, Badar A, Lythgoe MF, Årstad E. (2015) Bimodal Imaging of Inflammation with SPECT/CT and MRI Using Iodine-125 Labeled VCAM-1 Targeting Microparticle Conjugates. *Bioconj Chem*. 26,1542-1549.

23. Burtea C, Laurent S, Port M, Lancelot E, Ballet S, Rousseaux O, Toubeau G, Vander Elst L, Corot C, Muller RN. (2009) Magnetic Resonance Molecular Imaging of Vascular Cell Adhesion Molecule-1 Expression in Inflammatory Lesions Using a Peptide-Vectorized Paramagnetic Imaging Probe. *J Med Chem*. 52,4725-4742.

24. Bruckman MA, Jiang K, Simpson EJ, Randolph LN, Luyt LG, Yu X and Steinmetz NF. (2014) Dual-modal magnetic resonance and fluorescence imaging of atherosclerotic plaques in vivo using VCAM-1 targeted tobacco mosaic virus. *Nano Letters*. 14,1551-1558.

25. Al Faraja A, Luciani N, Kolosnjaj-Tabi J, Mattar E, Clement O, Wilhelm C and Gazeau F. (2013) Real-time high-resolution magnetic resonance tracking of macrophage subpopulations in a murine inflammation model: a pilot study with a commercially available cryogenic probe. *Contrast Media Mol Imaging*. 8,193-203.

26. Pillai R, Marinelli ER, Fan H, Nanjappan P, Song B, von Wronski MA, Cherkaoui S, Tardy I, Pochon S, Schneider M, Nunn AD, Swenson RE(2010) A Phospholipid-PEG2000 Conjugate of a Vascular Endothelial Growth Factor Receptor 2 (VEGFR2)-Targeting Heterodimer Peptide for Contrast-Enhanced Ultrasound Imaging of Angiogenesis. *Bioconjug Chem*. 21,556-562.

27. Merbach AS, Helm L, Toth E. (2013) The Chemistry of Contrast Agents in Medical Magnetic Resonance Imaging, 2nd Edition, *John Wiley and Sons Ed*.

28. Zhang S, Kovacs Z, Burgess S, Aime S, Terreno E, Sherry AD. (2001) {DOTA-bis(amide)}lanthanide Complexes: NMR Evidence for Differences in Water-Molecule Exchange Rates for Coordination Isomers. *Chem. Eur. J*. 7,288-296.

29. Delli Castelli D, Caligara MC, Botta M, Terreno E, Aime S. (2013) Combined high resolution NMR and 1H and 17O relaxometric study sheds light on the solution structure and dynamics of the lanthanide(III) complexes of HPDO3A. *Inorg Chem*. 52,7130-7138.

30. Troughton JS, Greenfield MT, Greenwood JM, Dumas S, Wiethoff AJ, Wang J, Spiller M, McMurry TJ, Caravan P. (2004) Synthesis and evaluation of a high relaxivity manganese(II)-based MRI contrast agent. *Inorg Chem*. 43,6313-6323.

31. Avedano S, Botta M, Haigh JS, Longo D, Woods M. (2013) Coupling fast water exchange to slow molecular tumbling in Gd^{3+} chelates: why faster is not always better. *Inorg. Chem.* 52,8436–8450.

32. Webber BC, Woods M. (2014) The confluence of structure and dynamics in lanthanide(III) chelates: how dynamics help define structure in solution. Dalton Trans. 43,251-258.

33. Caravan P, Farrar CT, Frullano L and Uppal R. (2009) Influence of molecular parameters and increasing magnetic field strength on relaxivity of gadolinium- and manganese-based T1 contrast agents. *Contrast Media Mol Imaging.* 4,89-100.

34. Helm L. (2010) Optimization of gadolinium-based MRI contrast agents for high magnetic-field applications. *Future Med Chem.* 2**,** 385-396.

35. Cittadino E, Ferraretto M, Torres E, Maiocchi A, Crielaard BJ, Lammers T, Storm G, Aime S andTerrenoE.(2012)MRI evaluation ofthe antitumor activity of paramagnetic liposomes loaded with prednisolone phosphate. *Eur J Pharm Sci*. 45,436-441.

36. Cittadino E, Botta M, Tei L, Kielar F, Stefania R, Chiavazza E, Aime S and Terreno E. (2013) In Vivo Magnetic Resonance Imaging Detection of Paramagnetic Liposomes Loaded with Amphiphilic Gadolinium(III) Complexes: Impact of Molecular Structure on Relaxivity and Excretion Efficiency. *ChemPlusChem*, 7,712-722.

37. Filippi M, Martinelli J, Mulas G, Ferraretto M, Teirlinck E, Botta M, Tei L, Terreno E. (2014) Dendrimersomes: a new vesicular nano-platform for MR-molecular imaging applications. *Chem Commun*. 50,3453-3456.

38. Qin SS, Yu ZW, Yu YX. (2009) Structural Characterization on the Gel to Liquid-Crystal Phase Transition of Fully Hydrated DSPC and DSPE Bilayers. *J. Phys. Chem. B*. 113,8114–8123.

39. Benetollo F, Bombieri G, Calabi L, Aime S, Botta M. (2003) Structural variations across the lanthanide series of macrocyclic DOTA complexes: insights into the design of contrast agents for magnetic resonance imaging. *Inorg. Chem.* 42,148−157.

40. Aime S, Barge A., Bruce JI, Botta M, Howard JAK, Moloney JM, Parker D, De Sousa AS, Woods M. (1999) NMR, Relaxometric, and Structural Studies of the Hydration and Exchange Dynamics of Cationic Lanthanide Complexes of Macrocyclic Tetraamide Ligands. J.*Am. Chem. Soc.* 121; 5762-5771.

41. Dunand FA, Aime S, Merbach AE. (2000) First ^{17}O NMR Observation of Coordinated Water on Both Isomers of $[Eu(DOTAM)(H_2O)]^{3+}$: A Direct Access to Water Exchange and its Role in the Isomerization. *J. Am. Chem. Soc*. 122,1506-1512.

42. Miller KJ, Saherwala AA, Webber BC, Wu Y, Sherry AD, Woods M. (2010) The Population of SAP and TSAP Isomers in Cyclen-Based Lanthanide(III) Chelates Is Substantially Affected by Solvent. *Inorg. Chem.* 49, 8662–8664.

43. Anelli PL, Lattuada L, Lorusso V, Schneider M, Tournier H, Uggeri F (2001), Mixed micelles containing lipophilic gadolinium complexes as MRA contrast agents, MAGMA. 114-20.

44. Vaccaro M, Mangiapia G, Paduano L, Gianolio E, Accardo A, Tesauro D and Morelli G. (2007) Structural and relaxometric characterization of peptide aggregates containing gadolinium complexes as potential selective contrast agents in MRI. *Chemphyschem*. 8,2526-38.